ARTICLE

Understanding Charge Transport in Wavy 2D Covalent Organic Frameworks

Received 00th January 20xx,
Accepted 00th January 20xx

DOI: 10.1039/x0xx00000x

Marta Martínez-Abadía,[a] Karol Strutyński,[b] Craig T. Stoppiello,[c,d] Belén Lerma Berlanga,[e] Carlos Martí-Gastaldo,[e] Andrei N. Khlobystov,[c,d] Akinori Saeki,[f] Manuel Melle-Franco,[b] and Aurelio Mateo-Alonso*[a,g]

Understanding charge transport in 2D covalent organic frameworks is crucial to increase their performance. Herein a new wavy 2D covalent organic framework has been designed, synthesized and studied to shine light on the structural factors that dominate charge transport.

Introduction

Covalent organic frameworks (COFs) are crystalline solids constituted of covalently linked organic monomers that have become promising materials for several applications, including gas separation and storage, liquid filtration and purification, heterogeneous catalysis and sensing, among others.[1] Among these, two-dimensional covalent organic frameworks (2D COFs) are constituted of crystalline stacks of COF layers. If these layers are formed by π-conjugated monomers, then interlayer π-stacking can open up optimal channels for charge and exciton transport,[2] enabling new opportunities to design crystalline materials for electronic and optoelectronic applications.[3]

In this regard, a strategy to increase π-orbital overlap between layers is the use of π-conjugated monomers with a large π-area, such as pyrene, phthalocyanine, tetrathiafulvalene, among many others.[4] Another strategy that has recently received attention relies on the use of monomers with distinct shapes (bowl-, propeller-, and armchair-shaped precursors)[5] that favour stacking between 2D COF layers.

Recently, we have introduced distorted polycyclic aromatic hydrocarbons as monomers for the synthesis of COFs with unusual architectures and properties.[6] The use of 2,3,10,11,18,19-hexahydroxy-*cata*-hexabenzocoronene (HBC, Figure 1) –an extended double-bowl shaped distorted polycyclic aromatic hydrocarbon– as nodes gave rise to 2D COFs with a wavy chair-like honeycomb lattice. The wavy structure of such 2D COF layers does not interfere with interlayer π-stacking between nodes and linkers but rather guided the stacking of additional layers by concave-convex self-complementarity. In consequence, the wavy 2D COF showed a high degree of crystallinity and charge transport properties similar to those of planar 2D COFs.

An important aspect of this type of wavy 2D COFs that remains to be understood and that have direct implications in the design of COFs with enhanced performance is to identify which units are directly involved in charge transport. For instance, both the HBC nodes and the (pyrene) linkers exhibit large π-areas and a high degree of π-stacking in the resulting wavy 2D COF. To answer this question, we have designed, synthesized and studied, a new wavy 2D COF where the pyrene linkers have been exchanged by benzene linkers (Marta-COF-2, Figure 2). Studies on Marta-COF-2 reveal that the columnar HBC π-stacks represents the primary pathway for charge transport in this family of wavy 2D COFs.

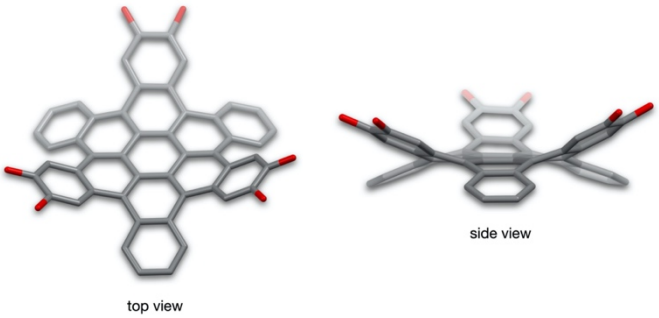

Figure 1. Crystal structure of HBC.[6]

[a] POLYMAT, University of the Basque Country UPV/EHU, Avenida de Tolosa 72, E-20018 Donostia-San Sebastian, Spain.
[b] CICECO - Aveiro Institute of Materials, Department of Chemistry, University of Aveiro, 3810-193 Aveiro, Portugal.
[c] School of Chemistry, University of Nottingham, University Park, Nottingham NG7 2RD, UK.
[d] The Nanoscale and Microscale Research Centre, University of Nottingham, University Park, Nottingham NG7 2RD, UK.
[e] Instituto de Ciencia Molecular, Universidad de Valencia, 46980 Paterna, Spain.
[f] Department of Applied Chemistry, Graduate School of Engineering, Osaka University, Suita, Osaka 565-0871, Japan.
[g] Ikerbasque, Basque Foundation for Science, Bilbao, Spain.
Email: amateo@polymat.eu

Electronic Supplementary Information (ESI) available. See DOI: 10.1039/x0xx00000x

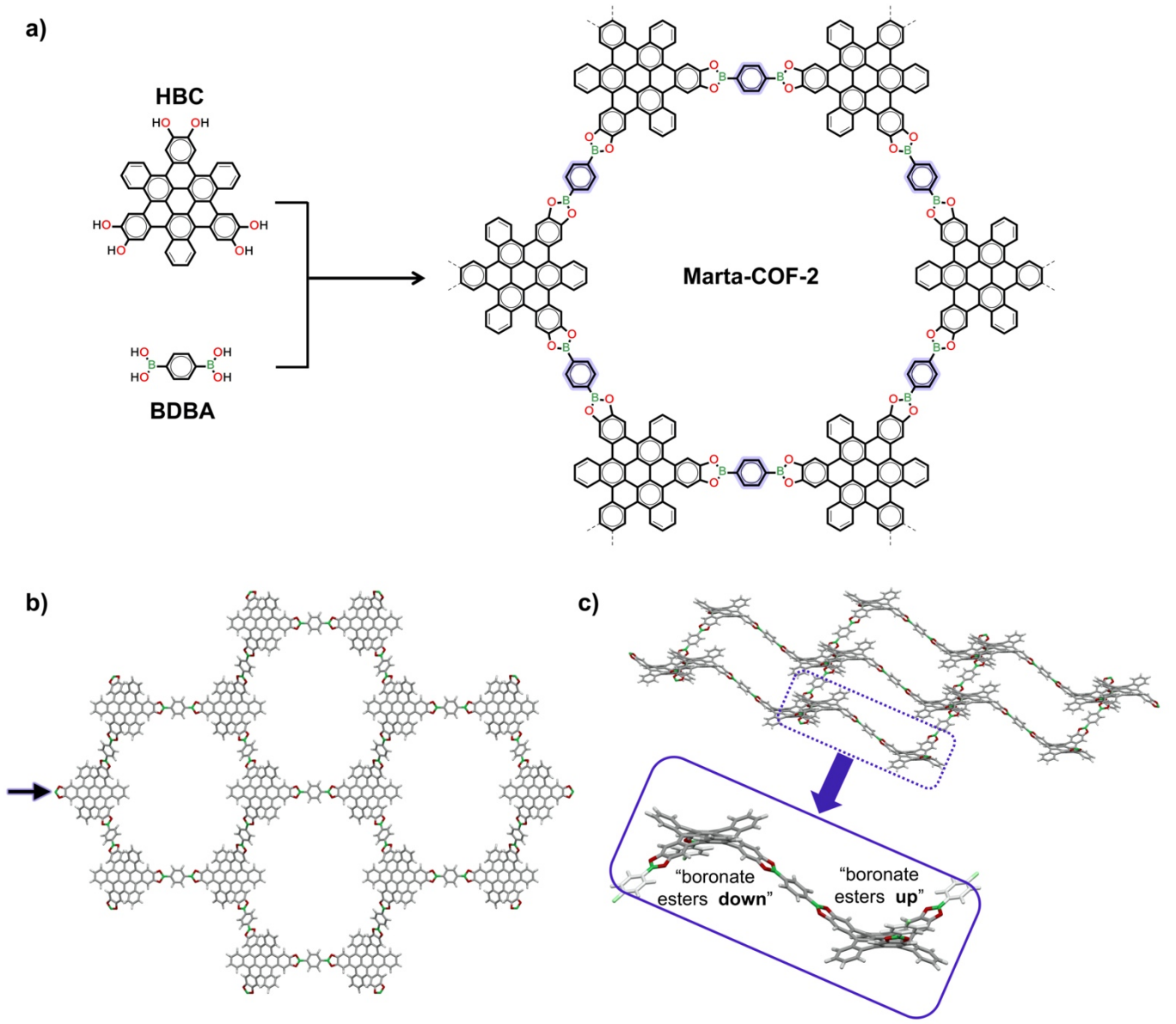

Figure 2. a) Schematic reaction for the synthesis of Marta-COF-2. b) Face-on and c) lateral view of the reconstructed monolayer structure of Marta-COF-2. The arrow in b) indicates the direction discussed in the microscopy section.

Results and discussion

Marta-COF-2 was synthesized by solvothermal condensation of 2,3,10,11,18,19-hexahydroxy-cata-hexabenzocoronene (HBC)[6] and benzene-1,4-diboronic acid (BDBA) in a mixture of 1,4-dioxane and mesitylene (2:1) at 120 °C for 72 hours in a sealed pre-scored ampoule (Figure 2a). Subsequently, the solid was isolated by filtration and washed with anhydrous tetrahydrofuran, acetone and hexane to provide Marta-COF-2 as a yellow solid (90% yield).

The Fourier-transform infrared (FT-IR) spectrum of Marta-COF-2 shows bands at 1334 and 1348 cm^{-1}, attributed to strong C-O stretching band distinctive for boronate ester five-membered rings, and the strong attenuation of hydroxyl groups from the precursors (Figure 3a). The Solid-State Cross Polarization Magic-Angle Spinning (SS CP/MAS) ^{13}C NMR spectrum of Marta-COF-2 (Figure 3b and S1) shows signals that correspond to the benzene and hexabenzocoronene residues, while the SS CP-MAS ^{11}B NMR spectrum (Figure 3c) shows a single peak characteristic of a single type of boronate ester linkage.

Marta-COF-2 exhibited clear diffraction peaks in the powder X-ray diffraction (PXRD) pattern (Figure 3d-e) with several resolved reflections. The monolayer and crystal structure of Marta-COF-2 were calculated using Density Functional Theory (DFT). Each layer is intrinsically undulated as consequence of the twisted and rigid structure of the HBC node and the alternated disposition of HBC nodes pointing above and below the plane, which gives rise to a chair-like honeycomb lattice (Figure 2b-c). The structural

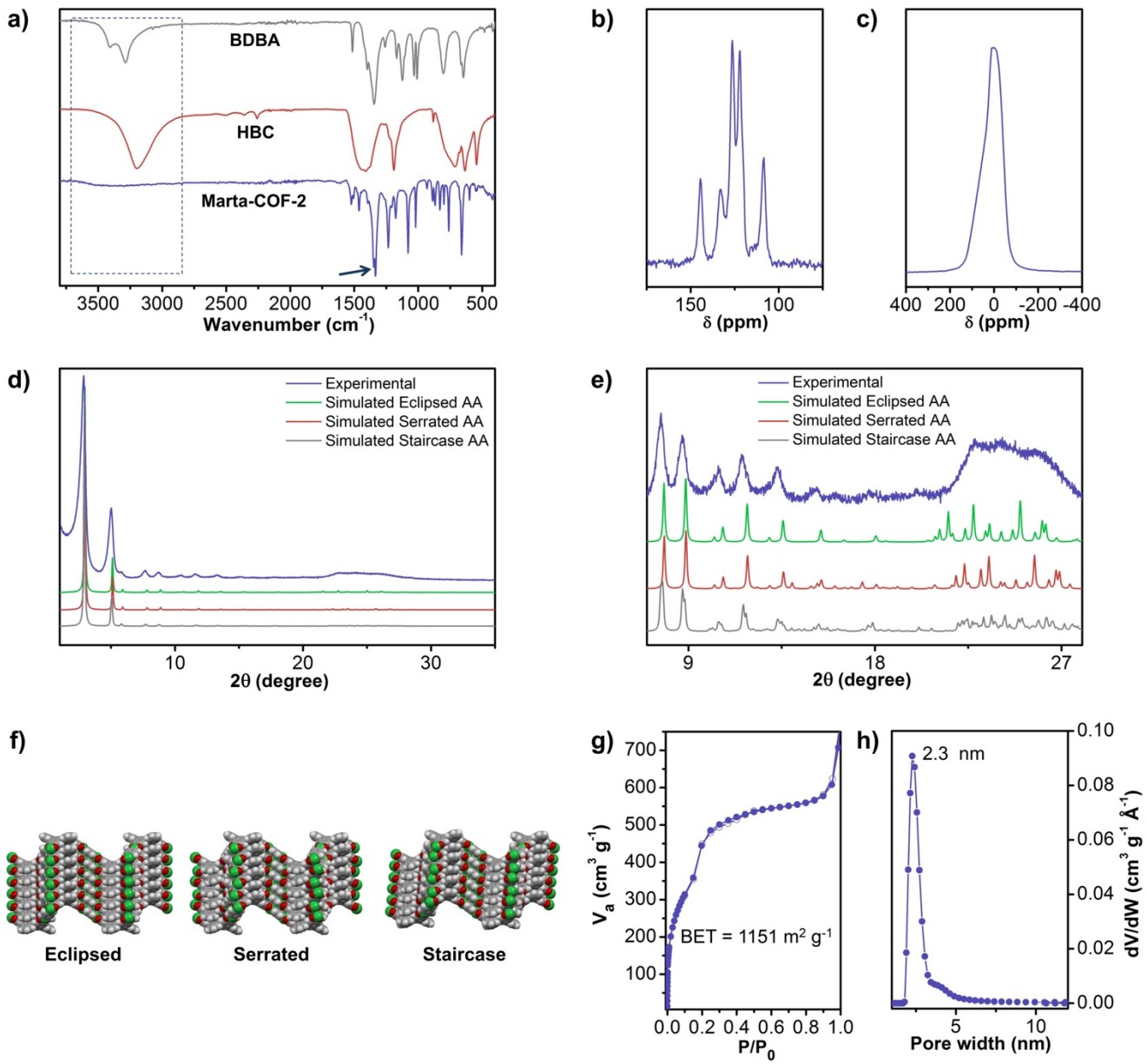

Figure 3. a) FTIR spectra of BDBA (grey), HBC (red) and Marta-COF-2 (blue). SS CP-MAS b) ^{13}C NMR (partial) and c) ^{11}B NMR of Marta-COF-2. d) Full and e) zoomed experimental and simulated PXRD patterns for the AA packing modes of Marta-COF-2. f) AA stacking modes of Marta-COF-2. g) Nitrogen adsorption and desorption isotherm profiles at 77 K and h) pore size distribution of Marta-COF-2.

concave-convex self-complementarity limits substantially the number of packing arrangements. Two general packing conformations (AA and AB) with three different interlayer stackings were computationally explored, namely, eclipsed, serrated and staircase (Figure 3f). First, the Binding Energy (BE) of the AB stacking modes shows systematically higher energy (~100 kcal/mol) than of the AA layer stacking modes (Table S1). Besides, the simulated PXRD diffractograms for AB packing modes do not fit with the experimental ones (Figure S2). Regarding AA stacking modes, the BE of the eclipsed AA stacking (–218 kcal/mol) is higher energy than those of the serrated and staircase AA layer stacking modes, which are similar in energy (–232 kcal/mol) (Table S1). This is also consistent with the simulated diffractograms of the serrated and staircase AA modes that show a better agreement with the experimental diffractograms than the eclipsed ones (Figure 3d-e), which is also consistent with recent experimental observations by Lotsch and co-workers.[7] Even if the predicted diffractograms cannot be used to preclude the presence of serrated AA stacking, the predicted PXRD pattern of the staircase AA configuration is more consistent with the experimental one. Pawley refinement (Figure S3) yielded unit cells nearly equivalent to the computational predictions (a = b = 35.05 Å, c = 8.13 Å, α = β = 90° and γ = 120°, R_p = 3.95% and R_{wp} = 8.11%). Additionally, the diffraction patterns at 2.86°, 5.02°, 5.83°, 7.67°, 8.70°, 10.49°, 11.59°, 13.29° were assigned

to the (100), (1$\bar{2}$0), (200), (210), (300), (310), (400) and (410) facets, respectively, of the staircase AA packing.

Marta-COF-2 exhibits a reversible type I nitrogen isotherm at 77 K (Figure 2g) with a microporous and mesoporous region. The Brunauer–Emmett–Teller (BET) surface area of 1151 $m^2 g^{-1}$ and a pore size of 2.3 nm (Figure 2h) calculated from the isotherm are consistent with theoretical values calculated for Marta-COF-2 in an AA stacking configuration (1400 $m^2 g^{-1}$ and 2.3 nm, Table S2).

High-resolution transmission electron microscopy (HR-TEM) revealed the presence of Marta-COF-2 crystallites that show channel-like features (Figures S4 and S5) that were attributed to the projection of the HBC columns across the zig-zag direction (see arrow in Figure 2b).

The charge transport properties of Marta-COF-2 were assessed by flash-photolysis time-resolved microwave conductivity (FP-TRMC).[8] FP-TRMC measures the pseudophotoconductivity ($\varphi\Sigma\mu$), which is directly related to the minimum or inherent charge carrier mobility of the material. The powders of Marta-COF-2 showed a $\varphi\Sigma\mu_{max}$ value of 0.5 × 10^{-4} cm^2 V^{-1} s^{-1}. This $\varphi\Sigma\mu_{max}$ value is in the same range as those generally observed on planar 2D COFs that oscillate between 10^{-5} and 10^{-4} cm^2 V^{-1} s^{-1}.[9] Most importantly, the $\varphi\Sigma\mu_{max}$ value of Marta-COF-2 is very similar to that observed on the equivalent wavy 2D COF with pyrene linkers ($\varphi\Sigma\mu_{max}$ = 0.6 × 10^{-4} cm^2 V^{-1} s^{-1}).[6] Taking into account that both wavy 2D COFs show virtually the same chair-like honeycomb 2D structure, the same packing configuration and the $\varphi\Sigma\mu_{max}$ values, we can safely conclude that the charge transport properties are nearly independent of the linker used (benzene and pyrene) and thus that charge transport takes place preferentially across the channels generated by the stacks of HBC nodes.

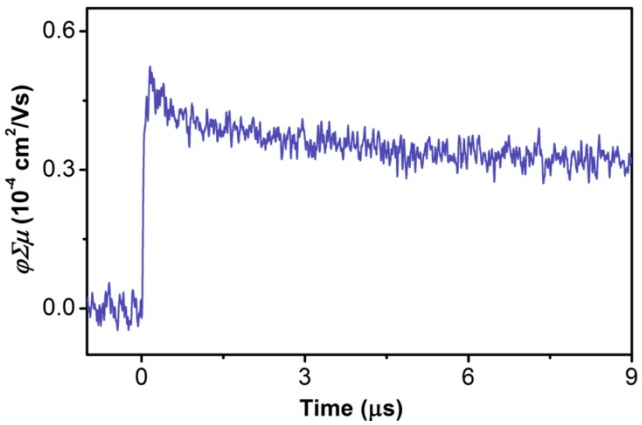

Figure 4. $\varphi\Sigma\mu$ transients of Marta-COF-2 measured by FP-TRMC.

Conclusions

In summary, we have designed and synthesized a new member of the wavy 2D COF family to shine light on the structural factors that influence their charge transport properties. Marta-COF-2 has been synthesized by condensation between a distorted HBC and BDBA and shows a chair-like honeycomb lattice with AA packing configuration as imposed by the wavy structure. The structure of Marta-COF-2 has been confirmed by a combination of FT-IR, SS NMR, PXRD, gas sorption and HR-TEM. FP-TRMC studies reveal that Marta-COF-2 shows a $\varphi\Sigma\mu_{max}$ value of 0.5 × 10^{-4} cm^2 V^{-1} s^{-1}, which is very similar to that of a structurally equivalent wavy 2D COF, which varies on the nature of the linkers, indicating that charge transport takes place preferentially across the stacks of HBC nodes. Our results illustrate that twisted aromatics are not only very useful structural units for the synthesis of COFs with unusual structures but also to control charge transport properties.

Author Contributions

M.M.-A. synthesized and characterized (FT-IR, NMR, PXRD) Marta-COF-2 under the supervision of A.M.-A.; K.S. carried out the simulations and constructed the different crystal structures under the supervision of M.M.-F.; C.T.S. and A.N.K. carried out and interpreted the transmission electron microscopy measurements; B.L.-B. and C.M.-G. carried out and interpreted the gas sorption measurements; A.S. carried out the FP-TRMC measurements; M.M.-A. and A.M.-A. wrote the manuscript with the contributions of all authors; A.M.-A. conceived and supervised the study.

Conflicts of interest

There are no conflicts to declare.

Acknowledgements

This work was carried out with support from the Basque Science Foundation for Science (Ikerbasque), POLYMAT, the University of the Basque Country (Grupo de Investigación GIU17/054), Gobierno de España (Ministerio de Ciencia e Innovación, Plan Estatal de Investigación Científica y Técnica y de Innovación 2017-2020), Gobierno Vasco (PIBA and BERC programmes) and acknowledge technical and human support provided by SGIker of UPV/EHU and European funding (ERDF and ESF). This project has received funding from the European Research Council (ERC) under the European Union's Horizon 2020 research and innovation programme (Grant Agreement No. 722951). In addition, support through the project IF/00894/2015 and within the scope of the project CICECO-Aveiro Institute of Materials, UIDB/50011/2020 & UIDP/50011/2020, financed by national funds through the Portuguese Foundation for Science and Technology/MCTES is gratefully acknowledged.

Notes and references

1. (a) A. P. Côté, A. I. Benin, N. W. Ockwig, M. O'Keeffe, A. J. Matzger and O. M. Yaghi, *Science*, 2005, **310**, 1166-1170; (b) C.-Y. Lin, D. Zhang, Z. Zhao and Z. Xia, *Adv. Mater.*, 2018, **30**, 1703646-1703661; (c) M. S. Lohse and T. Bein,

Adv. Funct. Mater., 2018, **28**, 1705553-1705623; (d) F. Zhao, H. Liu, S. D. R. Mathe, A. Dong and J. Zhang, *Nanomaterials*, 2018, **8**, 15-64; (e) X. Liu, D. Huang, C. Lai, G. Zeng, L. Qin, H. Wang, H. Yi, B. Li, S. Liu, M. Zhang, R. Deng, Y. Fu, L. Li, W. Xue and S. Chen, *Chem. Soc. Rev.*, 2019, **48**, 5266-5302; (f) S. J. Lyle, P. J. Waller and O. M. Yaghi, *Trends Chem.*, 2019, **1**, 172-184; (g) Y. Song, Q. Sun, B. Aguila and S. Ma, *Adv. Sci.*, 2019, **6**, 1801410-1801443; (h) K. Geng, T. He, R. Liu, S. Dalapati, K. T. Tan, Z. Li, S. Tao, Y. Gong, Q. Jiang and D. Jiang, *Chem. Rev.*, 2020, **120**, 8814-8933; (i) H. Wang, H. Wang, Z. Wang, L. Tang, G. Zeng, P. Xu, M. Chen, T. Xiong, C. Zhou, X. Li, D. Huang, Y. Zhu, Z. Wang and J. Tang, *Chem. Soc. Rev.*, 2020, **49**, 4135-4165; (j) Z. Wang, S. Zhang, Y. Chen, Z. Zhang and S. Ma, *Chem. Soc. Rev.*, 2020, **49**, 708-735; (k) F. Haase and B. V. Lotsch, *Chem. Soc. Rev.*, 2020.

2. (a) F. C. Grozema and L. D. A. Siebbeles, *Int. Rev. Phys. Chem.*, 2008, **27**, 87-138; (b) S. Patwardhan, A. A. Kocherzhenko, F. C. Grozema and L. D. A. Siebbeles, *J. Phys. Chem. C*, 2011, **115**, 11768-11772; (c) S. Jin, X. Ding, X. Feng, M. Supur, K. Furukawa, S. Takahashi, M. Addicoat, M. E. El-Khouly, T. Nakamura, S. Irle, S. Fukuzumi, A. Nagai and D. Jiang, *Angew. Chem. Int. Ed.*, 2013, **52**, 2017-2021; (d) A. Kuc, M. A. Springer, K. Batra, R. Juarez-Mosqueda, C. Wöll and T. Heine, *Adv. Funct. Mater.*, 2020, **30**, 1908004-1908020.

3. (a) M. A. Kumar, M. Javeed and B. Jong-Beom, *ChemNanoMat*, 2017, **3**, 373-391; (b) H. V. Babu, M. G. M. Bai and M. Rajeswara Rao, *ACS App. Mater. Interfaces*, 2019, **11**, 11029-11060; (c) M. D. Allendorf, R. Dong, X. Feng, S. Kaskel, D. Matoga and V. Stavila, *Chem. Rev.*, 2020, **120**, 8581-8640; (d) M. Souto, K. Strutyński, M. Melle-Franco and J. Rocha, *Chem. Eur. J.*, 2020, **26**, 10912-10935.

4. (a) E. Jin, Z. Lan, Q. Jiang, K. Geng, G. Li, X. Wang and D. Jiang, *Chem*, 2019, **5**, 1632-1647; (b) N. Huang, K. H. Lee, Y. Yue, X. Xu, S. Irle, Q. Jiang and D. Jiang, *Angew. Chem. Int. Ed.*, 2020, **59**, 16587-16593; (c) S. Cai, B. Sun, X. Li, Y. Yan, A. Navarro, A. Garzón-Ruiz, H. Mao, R. Chatterjee, J. Yano, C. Zhu, J. A. Reimer, S. Zheng, J. Fan, W. Zhang and Y. Liu, *ACS App. Mater. Interfaces*, 2020, **12**, 19054-19061.

5. (a) J.-T. Yu, Z. Chen, J. Sun, Z.-T. Huang and Q.-Y. Zheng, *J. Mater. Chem.*, 2012, **22**, 5369-5373; (b) L. Ascherl, T. Sick, J. T. Margraf, S. H. Lapidus, M. Calik, C. Hettstedt, K. Karaghiosoff, M. Döblinger, T. Clark, K. W. Chapman, F. Auras and T. Bein, *Nat. Chem.*, 2016, **8**, 310-316; (c) S. Dalapati, E. Jin, M. Addicoat, T. Heine and D. Jiang, *J. Am. Chem. Soc.*, 2016, **138**, 5797-5800; (d) F. Auras, L. Ascherl, A. H. Hakimioun, J. T. Margraf, F. C. Hanusch, S. Reuter, D. Bessinger, M. Döblinger, C. Hettstedt, K. Karaghiosoff, S. Herbert, P. Knochel, T. Clark and T. Bein, *J. Am. Chem. Soc.*, 2016, **138**, 16703-16710; (e) M. A. Belen, C.-L. Diego, P.-M. Iñigo, V. Giovanni, B. Alessandro, P. Jan, S. Karol, D. F. Steven, P. Francesco, M. Mario, K. A. N., M.-F. Manuel and M.-A. Aurelio, *Angew. Chem. Int. Ed.*, 2017, **56**, 6946-6951; (f) C. M. Thompson, G. Occhialini, G. T. McCandless, S. B. Alahakoon, V. Cameron, S. O. Nielsen and R. A. Smaldone, *J. Am. Chem. Soc.*, 2017, **139**, 10506-10513; (g) N. Keller, T. Sick, N. N. Bach, A. Koszalkowski, J. M. Rotter, D. D. Medina and T. Bein, *Nanoscale*, 2019, **11**, 23338-23345; (h) Z. Xie, B. Wang, Z. Yang, X. Yang, X. Yu, G. Xing, Y. Zhang and L. Chen, *Angew. Chem. Int. Ed.*, 2019, **58**, 15742-15746.

6. M. Martínez-Abadía, C. T. Stoppiello, K. Strutynski, B. Lerma-Berlanga, C. Martí-Gastaldo, A. Saeki, M. Melle-Franco, A. N. Khlobystov and A. Mateo-Alonso, *J. Am. Chem. Soc.*, 2019, **141**, 14403-14410.

7. A. M. Pütz, M. W. Terban, S. Bette, F. Haase, R. E. Dinnebier and B. V. Lotsch, *Chem. Sci.*, 2020, **11**, 12647-12654.

8. A. Saeki, Y. Koizumi, T. Aida and S. Seki, *Acc. Chem. Res.*, 2012, **45**, 1193-1202.

9. (a) S. Dalapati, M. Addicoat, S. Jin, T. Sakurai, J. Gao, H. Xu, S. Irle, S. Seki and D. Jiang, *Nat. Commun.*, 2015, **6**, 7786-7793; (b) H. Ding, Y. Li, H. Hu, Y. Sun, J. Wang, C. Wang, C. Wang, G. Zhang, B. Wang, W. Xu and D. Zhang, *Chem. Eur. J.*, 2014, **20**, 14614-14618; (c) S. Jin, T. Sakurai, T. Kowalczyk, S. Dalapati, F. Xu, H. Wei, X. Chen, J. Gao, S. Seki, S. Irle and D. Jiang, *Chem. Eur. J.*, 2014, **20**, 14608-14613; (d) X. Feng, L. Chen, Y. Honsho, O. Saengsawang, L. Liu, L. Wang, A. Saeki, S. Irle, S. Seki, Y. Dong and D. Jiang, *Adv. Mater.*, 2012, **24**, 3026-3031; (e) X. Feng, L. Liu, Y. Honsho, A. Saeki, S. Seki, S. Irle, Y. Dong, A. Nagai and D. Jiang, *Angew. Chem. Int. Ed.*, 2012, **51**, 2618-2622; (f) X. Ding, X. Feng, A. Saeki, S. Seki, A. Nagai and D. Jiang, *Chem. Commun.*, 2012, **48**, 8952-8954; (g) S. Wan, F. Gándara, A. Asano, H. Furukawa, A. Saeki, S. K. Dey, L. Liao, M. W. Ambrogio, Y. Y. Botros, X. Duan, S. Seki, J. F. Stoddart and O. M. Yaghi, *Chem. Mater.*, 2011, **23**, 4094-4097; (h) X. Ding, J. Guo, X. Feng, Y. Honsho, J. Guo, S. Seki, P. Maitarad, A. Saeki, S. Nagase and D. Jiang, *Angew. Chem. Int. Ed.*, 2011, **50**, 1289-1293; (i) X. Ding, L. Chen, Y. Honsho, X. Feng, O. Saengsawang, J. Guo, A. Saeki, S. Seki, S. Irle, S. Nagase, V. Parasuk and D. Jiang, *J. Am. Chem. Soc.*, 2011, **133**, 14510-14513.

Supporting Information

Understanding Charge Transport in Wavy Two-Dimensional Covalent Organic Frameworks

Marta Martínez-Abadía,[a] Karol Strutyński,[b] Craig T. Stoppiello,[c,d] Belén Lerma Berlanga,[e] Carlos Martí-Gastaldo,[e] Andrei N. Khlobystov,[c,d] Akinori Saeki,[f] Manuel Melle-Franco,[b] and Aurelio Mateo-Alonso*[a,g]

[a] *POLYMAT, University of the Basque Country UPV/EHU, Avenida de Tolosa 72, E-20018 Donostia-San Sebastian, Spain.*

[b] *CICECO - Aveiro Institute of Materials, Department of Chemistry, University of Aveiro, 3810-193 Aveiro, Portugal.*

[c] *School of Chemistry, University of Nottingham, University Park, Nottingham NG7 2RD, UK.*

[d] *The Nanoscale and Microscale Research Centre, University of Nottingham, University Park, Nottingham NG7 2RD, UK.*

[e] *Instituto de Ciencia Molecular, Universidad de Valencia, 46980 Paterna, Spain.*

[f] *Department of Applied Chemistry, Graduate School of Engineering, Osaka University, Suita, Osaka 565-0871, Japan.*

[g] *Ikerbasque, Basque Foundation for Science, Bilbao, Spain.*

Email: amateo@polymat.eu;

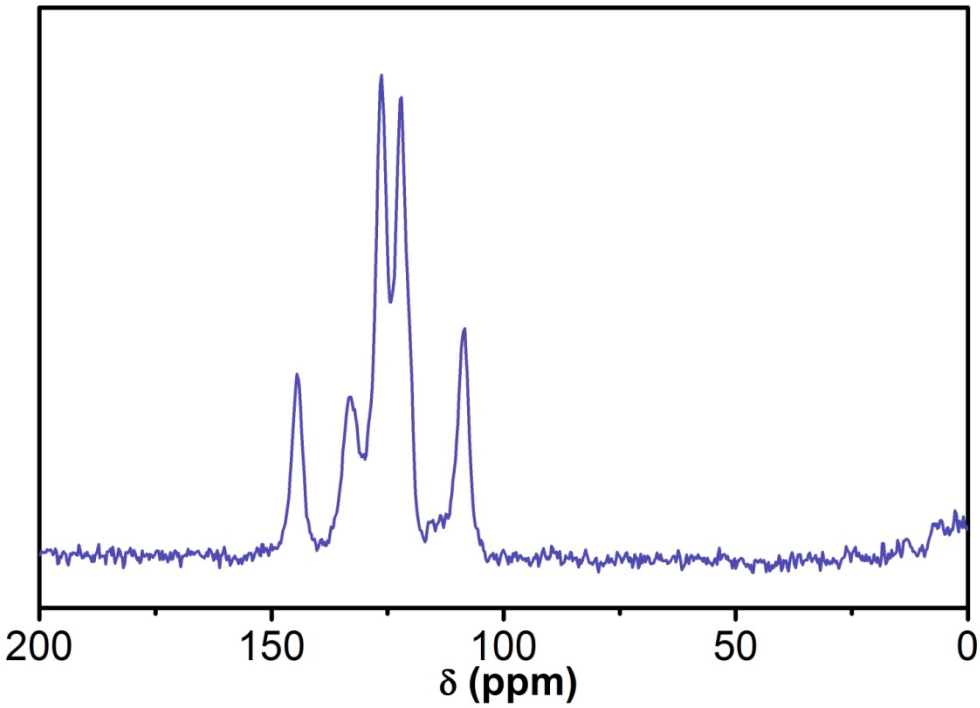

Figure S1. SS ^{13}C NMR Spectrum of Marta-COF-2.

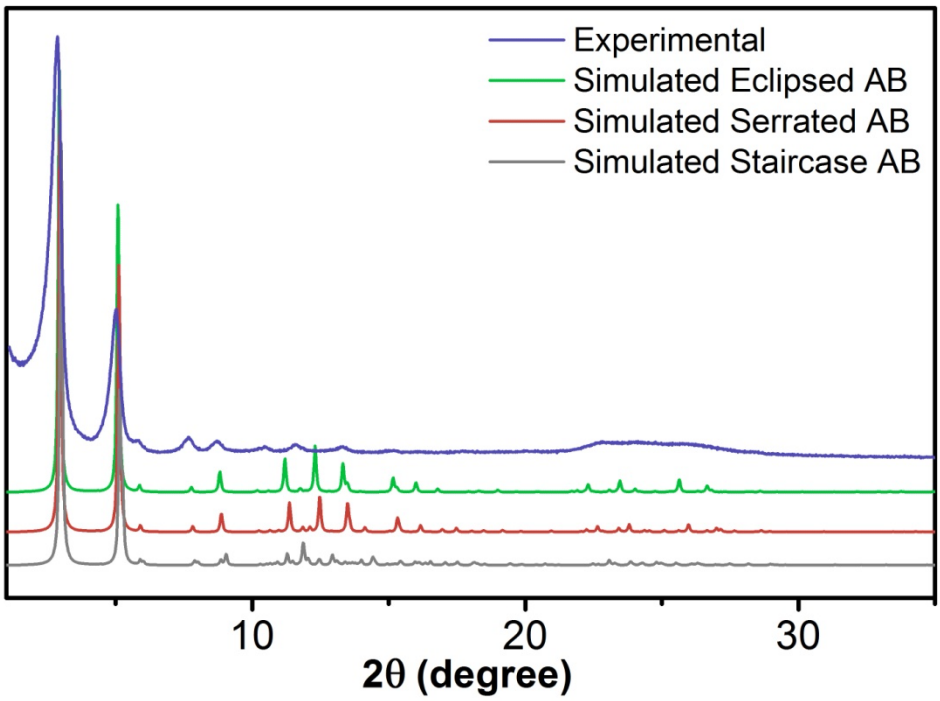

Figure S2. Experimental PXRD pattern (blue line), simulated diffraction PXRD pattern for the simulated perfectly eclipsed AB (green line), serrated AB (red line) and staircase AB (grey line) stacking of Marta-COF-2.

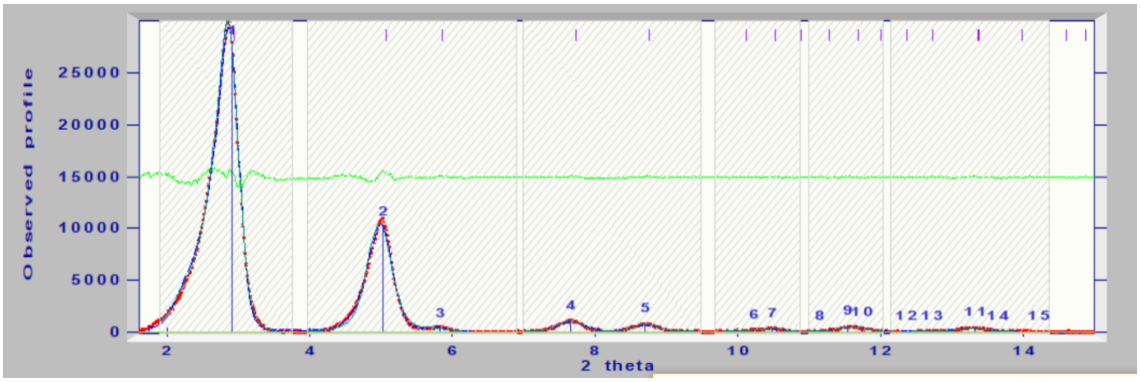

Figure S3. PXRD analysis for Marta-COF-2 including the experimental diffraction pattern (red dashed line), Pawley refined pattern (blue line), and the difference between the refined and experimental pattern (green line).

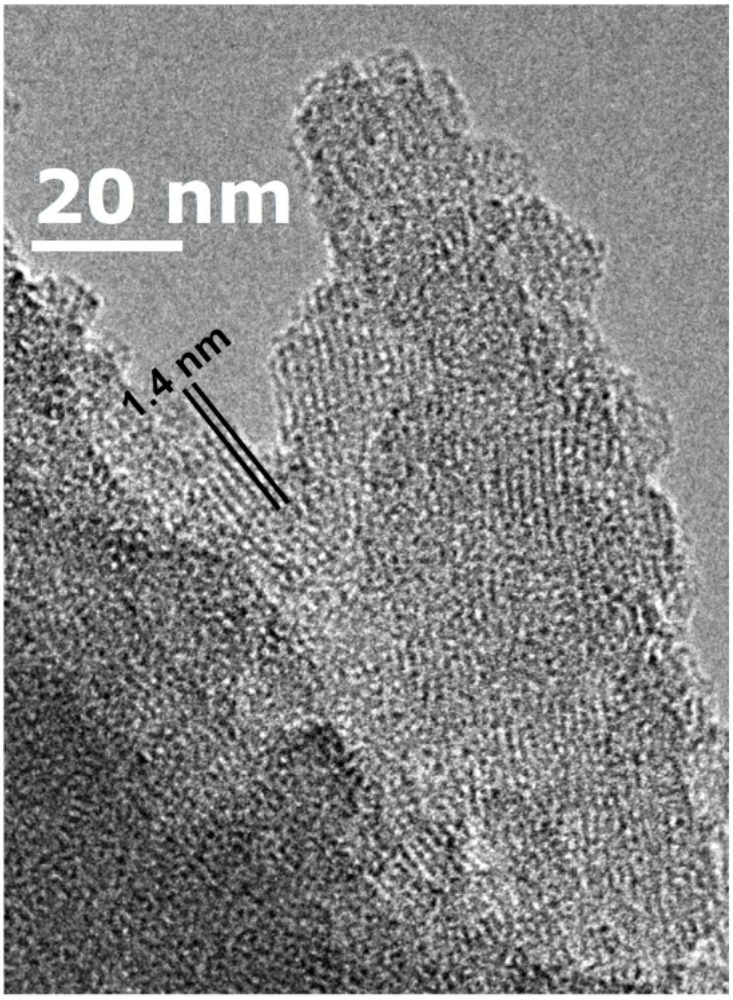

Figure S4. HR-TEM image of Marta-COF-2.

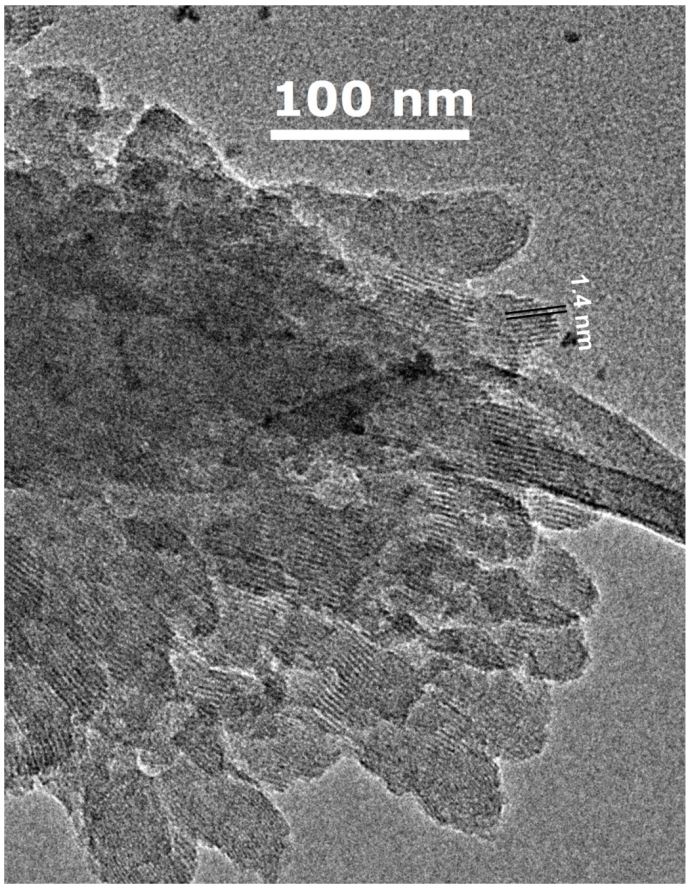

Figure S5. HR-TEM image of Marta-COF-2.

Table S1. Binding energies (BE) and gap of Marta-COF-2 obtained from DFT calculations.

System	Average ab	c	E	B3LYP Gap	BE
	Å	Å	eV	eV	kcal/mol
Monolayer	34.41	100.00	-147526.31	3.17	
AA full eclipsed	34.45	8.49	-295062.20	2.83	-218
AA serrated	34.40	8.18	-295062.79	2.61	-232
AA staircase	34.77	8.09	-295062.81	2.72	-232
AB full eclipsed	34.67	8.18	-295057.97	2.75	-121
AB serrated	34.45	8.06	-295058.20	2.78	-126
AB staircase	34.57	7.90	-295058.37	2.76	-130

Table S2. Porosity data for Marta-COF-2. The porosity, surface area and internal volume of predicted structures was calculated using PoreBlazer v4.0, with 1000 samples per atom and 0.2 Å spatial resolution.

Conformation	Density	Pore size	Surface Area	Surface Area	Probe-occupiable Volume
	g/cm^3	Å	m^2/g	m^2/cm^3	cm^3/g
AA full eclipsed	0.635	23.690	1455	924	0.929
AA serrated	0.661	22.900	1394	921	0.877
AA staircase	0.648	23.180	1400	908	0.910
AB full eclipsed	0.650	6.980	2625	1707	0.950
AB serrated	0.669	7.670	2334	1560	0.899
AB staircase	0.698	8.580	1959	1368	0.801

Experimental procedures

Reagents for synthesis were, if not otherwise specified, purchased from Aldrich, TCI or Acros Organics. Column chromatography was carried out using Silica gel 60 (40-60 μm) from Scharlab. Analytical thin layer chromatography (TLC) was done using aluminum sheets (20x20 cm) pre-coated with silica gel RP-18W 60 F254 from Merck. UV-active compounds were detected with a UV-lamp from CAMAG at wavelength λ = 254 or 366 nm. HBC was synthesized according to reported methods.[1] Marta-COF-2 was synthesized in a pre-scored 5 mL ampoule from Aldrich. For its synthesis and purification anhydrous 1,4-dioxane (99.8%), anhydrous acetone (99.8%), anhydrous hexane (97%) were purchased from Acros Organics. THF was dried using an Innovative Pure Solve solvent purification system and mesitylene (97%) was obtained from Acros Organics and dried with molecular sieves.

Solid-State ^{1}H, ^{11}B and ^{13}C CP/MAS NMR spectra were recorded on a Bruker Avance III 400 MHz NMR spectrometer at a MAS rate of 12 kHz and a CP contact time of 2 ms.

ATR-FTIR spectra were recorded on a Bruker ALPHA ATR-IR spectrometer.

The powder X-ray diffraction (PXRD) patterns were collected by using a PHILIPS X'PERT PRO automatic diffractometer operating at 40 kV and 40 mA, in theta-theta configuration, secondary monochromator with Cu-Kα radiation (λ = 1.5418 Å) and a PIXcel solid state detector (active length in 2θ 3.347º). Data were collected from 1 to 50° 2θ (step size = 0.026 and time per step = 300 s, total time 40 min) at room temperature. A variable divergence slit, giving a constant 4.0 mm area of sample illumination, was used.

The pore structure was evaluated by nitrogen sorption isotherms, measured at 77 K with a Micromeritics 3Flex apparatus. The samples were degassed in an Autosorb station at and 10^{-6} Torr at 100 °C prior to analysis. Surface area, pore size and volume values were calculated from nitrogen adsorption-desorption isotherms (77 K). Specific surface area (SA) was calculated by multi-point Brunauer-Emmett-Teller (BET) method. Total pore volume was taken at P/P_0=0.96. Pore size distribution was analysed for the adsoption branch by using classical methods and a cylindrical pore model.

Electron Microscopy. All samples were prepared by dispersion in acetone and drop cast onto lacey carbon-coated copper TEM grids (Agar). High Resolution Transmission Electron Microscopy (HRTEM) analysis was performed on a JEOL2100F operating at 200 kV. The morphology of the samples was determined by taking low magnification (ca. x 30k mag) images from different regions of the specimen, and the nanoscale features were imaged using high resolution imaging (ca. x 100k mag).

FP-TRMC experiments were conducted for the sample on a quartz plate using the third harmonic generator (THG; 355 nm) of a Nd:YAG laser (Continuum Inc., Surelite II, 5–8 ns pulse duration, 10 Hz) as the excitation source (9.1×10^{15} photons cm^{-2} $pulse^{-1}$). The frequency and power of microwave were ~9.1 GHz and 3 mW, respectively. The photoconductivity transient $\Delta\sigma$ was converted to the product of the quantum yield (φ) and the sum of charge carrier mobilities $\sum\mu$ ($= \mu_+ + \mu_-$) by the formula $\varphi\sum\mu = \Delta\sigma(eI_0F_{light})^{-1}$, where e and F_{light} are the unit charge of a single electron and a correction (or filling) factor, respectively.

Synthesis and characterization

Marta-COF-2: HBC (25.42 mg, 0.0364 mmol) and benzene-1,4-diboronic acid (9.03 mg, 0.0545 mmol) were sonicated in a mixture of degassed 1,4-dioxane/mesitylene (2:1, 2.25 mL) in a pre-scored 5 mL ampoule under nitrogen. The suspension was degassed by using three freeze-pump-thaw cycles, and the ampoule was sealed off using flame and heated at 125 ºC for 3 days. Marta-COF-2 was obtained as a yellow solid (28 mg, 90 % yield), which was collected by filtration and washed five times with anhydrous tetrahydrofurane, acetone and hexane. The powder was dried at 30 ºC under vacuum for 24 hours. SS ^{1}H-NMR (δ) (ppm): 6.97. SS ^{13}C-NMR (δ) (ppm): 144.4, 133.1, 126.4, 122.1, 108.5. SS ^{11}B-NMR (δ) (ppm): 3.32 ppm. ATR-FTIR (cm^{-1}): 1522, 1462, 1348, 1334, 1234.

Modelling and predicting electronic properties

Two methods were applied to study the structure and electronic properties of Marta-COF-2: Density Functional Theory (DFT) and semi-empirical Density Functional Theory Tight Binding (TB). In order to include van der Waals interactions we used state of the art, range separated MBD@rsSCS correction on top of the PBE functional.[2,3] DFT calculations were performed with the Fritz Haber Institute *ab initio* molecular simulations (FHI-aims) package using "light" numeric atomic orbitals, which approximately correspond to TZVP level of calculations.[3-7]

Two general packing conformations, AA and AB, with three different interlayer stackings were investigated, namely: eclipsed, serrated and staircase, see Figure S6.

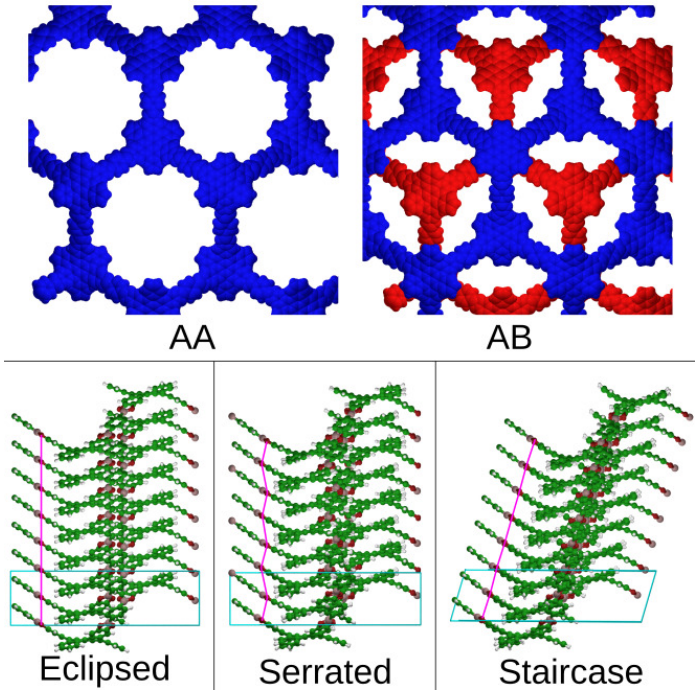

Figure S6. Conformations of Marta-COF-2. General structure (top) and possible stacking of the layers (bottom). Pink line indicates how equivalent atoms in different layers are stacked.

References

1. M. Martínez-Abadía, C. T. Stoppiello, K. Strutynski, B. Lerma-Berlanga, C. Martí-Gastaldo, A. Saeki, M. Melle-Franco, A. N. Khlobystov and A. Mateo-Alonso, A Wavy Two-Dimensional Covalent Organic Framework from Core-Twisted Polycyclic Aromatic Hydrocarbons. *J. Am. Chem. Soc.* 2019, **141**, 14403-14410.
2. Tkatchenko, A.; DiStasio, R. A.; Car, R.; Scheffler, M. Accurate and Efficient Method for Many-Body van Der Waals Interactions. *Phys. Rev. Lett.* 2012, **108**, 236402.
3. Tkatchenko, A.; Scheffler, M. Accurate Molecular Van Der Waals Interactions from Ground-State Electron Density and Free-Atom Reference Data. *Phys. Rev. Lett.* 2009, **102**, 073005.
4. Blum, V.; Gehrke, R.; Hanke, F.; Havu, P.; Havu, V.; Ren, X.; Reuter, K.; Scheffler, M. Ab Initio Molecular Simulations with Numeric Atom-Centered Orbitals. *Comput. Phys. Commun.* 2009, **180**, 2175–2196.
5. Marek, A.; Blum, V.; Johanni, R.; Havu, V.; Lang, B.; Auckenthaler, T.; Heinecke, A.; Bungartz, H.-J.; Lederer, H. The ELPA Library: Scalable Parallel Eigenvalue Solutions for Electronic Structure Theory and Computational Science. *J. Phys. Condens. Matter* 2014, **26**, 213201.
6. Yu, V. W.; Corsetti, F.; García, A.; Huhn, W. P.; Jacquelin, M.; Jia, W.; Lange, B.; Lin, L.; Lu, J.; Mi, W.; et al. ELSI: A Unified Software Interface for Kohn–Sham Electronic Structure Solvers. *Comput. Phys. Commun.* 2018, **222**, 267–285.
7. Lejaeghere, K.; Bihlmayer, G.; Björkman, T.; Blaha, P.; Blügel, S.; Blum, V.; Caliste, D.; Castelli, I. E.; Clark, S. J.; Corso, A. D.; et al. Reproducibility in Density Functional Theory Calculations of Solids. *Science* 2016, **351**, aad3000.